

## **Isothermal models of gas-turbine combustors**

**By A. S. GREEN† AND J. H. WHITELAW**

Department of Mechanical Engineering, Imperial College, London SW7 2BT

(Received 10 November 1981)

Measurements of mean axial velocity have been obtained in two perspex models which simulate important features of gas-turbine combustors and are compared with calculations based on the numerical solution of the three-dimensional equations that represent conservation of mass and momentum. The measurements show, for example, the effect of primary jet trajectory on the magnitude and proportion of total mass flow contained in the primary vortex. They also allow the value of the calculation method to be appraised and, in this context, it is shown that the local velocity values are subject to large errors in small regions of the flow but important parameters, such as the length of the primary vortex, are represented more than adequately for engineering purposes. Errors due to numerical approximations appear to be at least as important as those due to the two-equation turbulence model used to represent turbulent features of the flow.

---

### **1. Introductory remarks**

Experiments with water models of gas-turbine combustors have been used for many years as simple and comparatively cheap means of supporting design. In general, the measurements have been based on flow visualization in perspex replicas of real combustors, and the information obtained has been necessarily qualitative. The present measurements were also obtained in perspex models, but the models were simplified to allow the examination of specific boundary conditions, and the results are quantitative. They are supported by calculated results which, by comparison with the measurements, allow appraisal of the calculation method and add information for boundary conditions outside the range of the measurements. The longer-term purpose is to develop and test a calculation method that will aid the design process and reduce the number of measurements necessary with model and real combustion chambers.

Several recent papers (e.g. Jones & McGuirk 1980*a*; Harsha 1981) have referred to the possible design advantages to be gained from the development of methods for the numerical solution of differential equations representing conservation of mass, momentum, enthalpy and species with boundary conditions corresponding to combustor geometries. A substantial literature now exists on the subject on combustion modelling (see e.g. Libby & Williams 1980; Jones & Whitelaw 1982), but it is clear from the latter paper that the problems associated with numerical and turbulence assumptions are in many situations, and particularly where heat-transfer properties and major species are of interest, more important than those associated with combustion models. The calculations presented here help to quantify these uncertainties for isothermal flows and to provide information on the relative importance of numerical and turbulence-model errors.

† Present address: Atkins Research and Development, Epsom, Surrey, U.K.

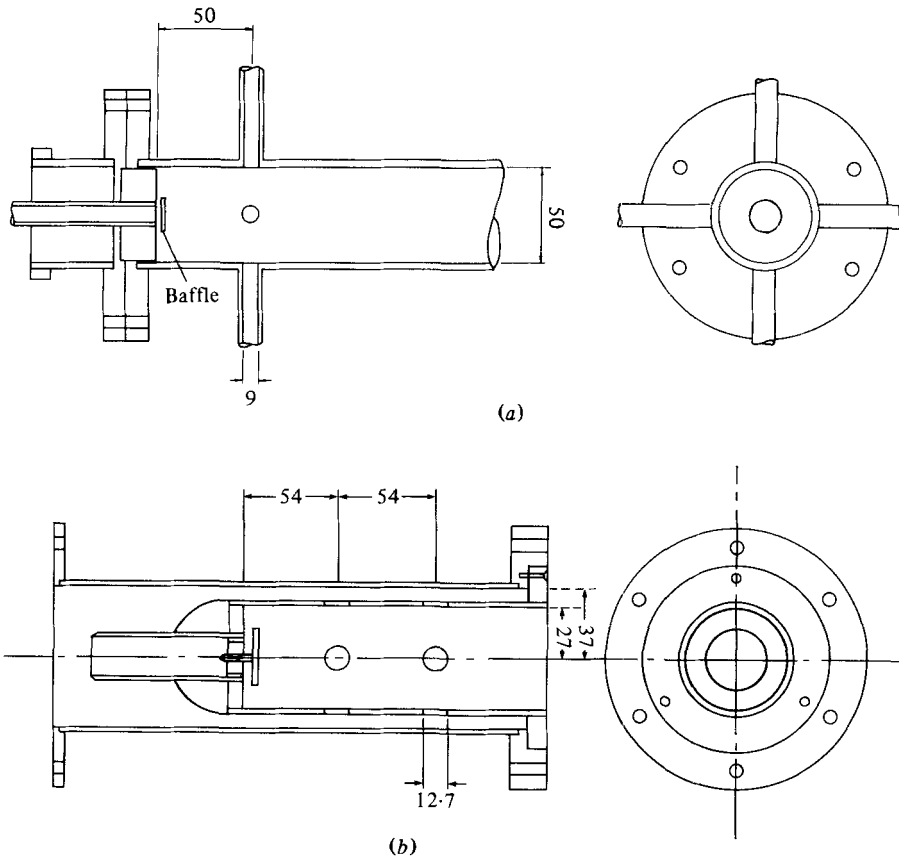


FIGURE 1. The three-dimensional models: (a) without and (b) with an annulus.

Two geometrical configurations, shown in figure 1, were used for the present investigations. The geometry of figure 1(a) comprised four radial jets, with  $90^\circ$  separation around the circumference of a perspex tube, and a single axial jet with a baffle located immediately downstream of the baseplate. The much-simplified inlet conditions, as compared with a real combustor, comprised a radial jet from behind the baffle, simulating a typical fuel-inlet device, and four fixed-angle primary jets. Although idealized, most of the main aerodynamic features of a real combustor are simulated and provide a severe test of the assumptions inherent in any calculation method. The geometry of figure 1(b) comprised the same elements as those of the first geometry, together with additional features that increase the complexity of the flow and its measurement and calculation. These include the entry of primary jets through circular holes supplied from an annulus, and secondary jets – a second set of four circular holes – through which cooling air is admitted in real combustors.

Preliminary investigations, using flow visualization, were carried out to establish the nature of the flow for both geometries. Detailed and quantitative measurements of the axial velocity were then obtained with a laser-Doppler anemometer and, with symmetry established, are presented for a radial plane through hole centres and for a radial plane midway, i.e.  $45^\circ$ , between hole centres. Calculated results were obtained for a symmetrical sector of each geometry and the magnitude of probable uncertainties established by comparison with the measurements. Further calculations were made

to demonstrate the influence of the ratio of mass flows through the radial and axial jets and the influence of radial-jet trajectory.

The experimental and computational investigations are described and results presented in §§2 and 3. The laser-Doppler anemometer and the numerical procedure of the calculation method are described briefly in order to allow their essential features to be identified and to aid the assessment of accuracy. Further details are available in the references cited.

## 2. Experimental investigation

The model combustor of figure 1 (*a*) comprised a 50 mm inside-diameter perspex tube with four 9 mm inside-diameter pipes symmetrically located with their centre-lines 50 mm downstream of the exit plane of a fifth 9 mm diameter hole. A 19 mm diameter baffle was located downstream of the exit plane of the axial hole, and local velocity measurements were obtained with flow rates of 0.151 and 0.774 kg/s in the axial and radial jets respectively, and with a Reynolds number based on the bulk axial velocity in the downstream region of the 50 mm tube of  $4.7 \times 10^4$ .

The second model combustor (figure 1 *b*) comprised a tube of inside diameter 74 mm, which formed the outer wall of an annulus, and a model flame tube, which was secured at its downstream end so as to form a symmetric annulus of 7 mm gap. In common with the more-idealized arrangement of figure 1 (*a*), a centrally located axial hole and baffle simulated a fuel-vaporizer inlet; in this case, however, two sets of equispaced 12.7 mm diameter holes represented primary and dilution holes. The central tube was connected to the upstream side of the baseplate to supply the axial jet: the balance of the water flow entered the chamber through the annulus, which was blocked at its downstream end, and through the primary and dilution holes. Measurements were obtained with mass flows of 0.47 and 1.77 kg/s in the central tube and annulus respectively to give a Reynolds number of  $5.3 \times 10^4$ . The division of the annulus flow between the primary and dilution jets was found to be equal within measurement accuracy.

Both models could be rotated to allow measurements of the axial component of mean velocity in different planes with a laser-Doppler anemometer. The optical components of the anemometer comprised a 5 mW helium-neon laser, a rotating diffraction grating to divide the incident light beam and provide frequency shift up to 3 MHz between the two first-order beams, a light-collection arrangement and a photomultiplier (EMI9558). The Doppler signals obtained from contaminant particles in the water were processed with a frequency-tracking demodulator (Cambridge Consultants CC01). Similar instrumentation was used for the measurements of Green & Whitelaw (1980) and allowed the measurement of components of mean velocity and the r.m.s. of the corresponding fluctuations with precision of  $\pm 2$  and  $\pm 5$  % respectively. Further comments on instrumentation of this type have been provided, for example, by Durst, Melling & Whitelaw (1981).

Preliminary measurements were made to evaluate the symmetry of the three flows. The mass flow through each of the four radial pipes was made equal within the accuracy of the anemometer, i.e. to better than 2 %. The flow in each of the four pipes was turbulent with boundary layers of less than 15 % of the diameter at the measurement location, which was one pipe diameter upstream of the exit plane. In the 50 mm pipe, measurements across diameters where symmetry should exist revealed deviations of not more than 5 % in the downstream flow: larger deviations from symmetry were noted in the low-velocity flow within the upstream recirculation,

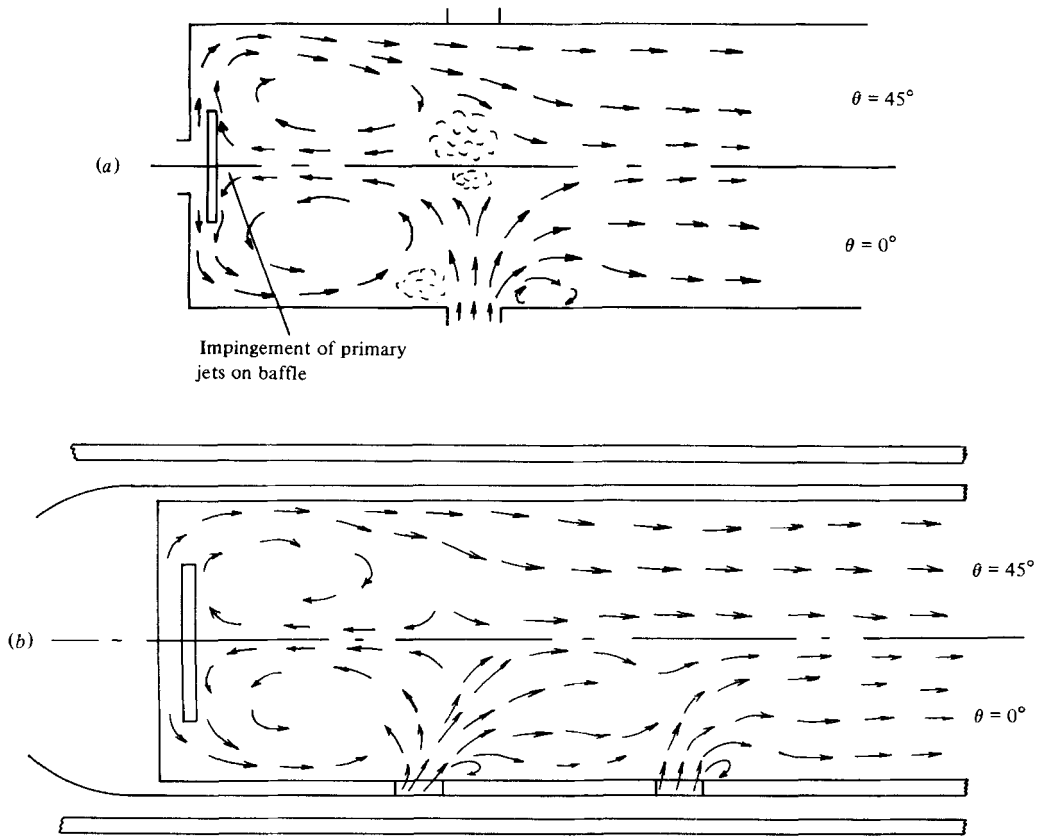


FIGURE 2. Flow visualizations of (a) non-annulus geometry and (b) annulus geometry.

but did not exceed 15% of the measured local velocity values. Symmetry tests were carried out with the geometry of figure 1 (b) and yielded similar results, even though the flow to the radial holes could not be independently controlled.

Flow visualization of hydrogen bubbles revealed flow patterns which have been indicated diagrammatically in figure 2 with precision similar to that obtained in the traditional water-model experiment used for development purposes. The figure shows that the flow from the radial jets contributes to the primary-region flow and that the large toroidal vortex, which has nearly the same dimensions in the  $0^\circ$  and  $45^\circ$  planes, provides the mixing and residence time required for proper combustion. It is clear from figure 2 (a), and additional studies, that the baffle reduces almost to zero the dependence of the length of the primary toroidal vortex on the ratio of primary to radial jet velocities.

As can be seen from figure 2 (b), the flow in the annulus exits from the radial holes with a trajectory which is angled in the downstream region, presumably with the consequence that a smaller proportion of the primary-jet fluid contributes to the upstream vortex. Owing to the larger mass flow in the annulus upstream of the primary jets, the trajectory angle of the primary jets is shallower than that of the secondary jets. Consequently fluid from the upstream region is less able to flow around the jets and into the separation region.

Measurements of mean axial velocity were obtained with the geometry of figure

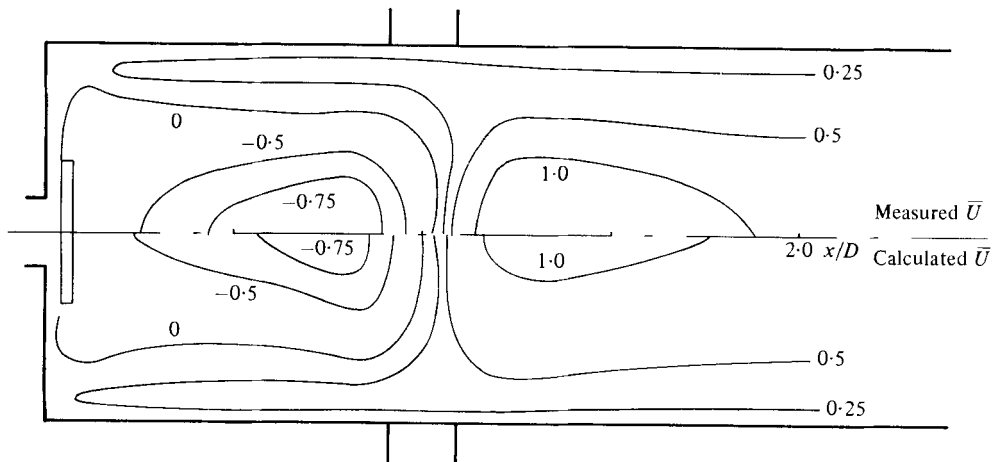


FIGURE 3. Comparison of calculated and measured mean axial velocity contours of case 1 ( $\theta = 45^\circ$ ).

1(a) and corresponding contours, based on measurements at twelve axial and nine radial measuring locations on the  $45^\circ$  plane, are shown on figure 3. The corresponding calculated velocity contours are also shown on this figure and are discussed later. In this case, the average velocity of the water in the radial tubes is 3 m/s and in the axial tube the bulk velocity is 0.6 m/s. Thus, the ratio of radial jet to maximum cross-flow velocity is at least 5. An implication is that the shape of the velocity profile in the exit plane of the jets may not be an important parameter in corresponding calculations where long radial tubes are present. The velocity profile could not be measured in the exit plane but, at 1.5 pipe diameters upstream, the profile was symmetric within 5% of the maximum velocity.

The maximum negative velocity is approximately 1.1 m/s with a maximum positive velocity of approximately 1.7 m/s and these values occur close to the centreline and at  $x/D = 0.8$  and  $1.2$  respectively. Although measurements were not obtained in the region of the jet on the zero-degree plane, these maximum velocity values provide an indication of the division of jet fluid between upstream and downstream directions. The normal-stress profiles were also measured and proved to be comparatively uniform in the upstream region. The jet mixing tended to cause higher values closer to the axis, and this was evident immediately upstream and downstream of the axial plane of the radial jets. Further details have been reported by Green (1981).

Similar measurements were made for a number of ratios of the mass flow through the axial and radial jets. A 30% reduction in the axial-jet mass flow proved to have little effect on the downstream flow. A 90% reduction in the radial-jet mass flow also led to a generally similar flow pattern, although the contour of zero velocity in the primary zone changed from near-radial as in figure 3, to allow a region of positive velocity at  $x/D = 1$  that was twice as large as that at  $x/D = 0.1$ . In addition, the maximum negative velocity occurred at  $x/D = 0.4$  rather than at  $x/D = 0.8$ .

Similar measurements of mean axial velocity were obtained in the model combustor of figure 1(b), and corresponding contours are shown in figure 4 for both the  $0^\circ$  plane and the  $45^\circ$  plane. The average velocity of the water passing through the head of the model combustor is 1.0 m/s and through each of the primary and secondary jets

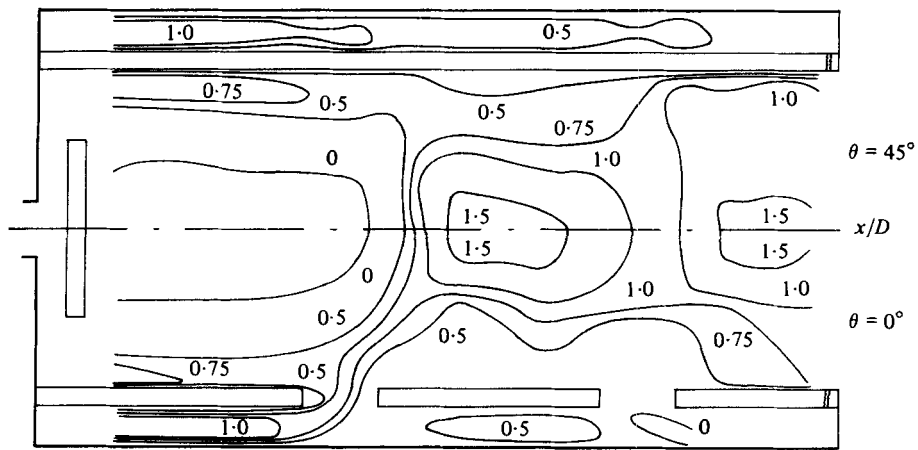


FIGURE 4. Measured mean axial velocity contours for  $\theta = 0^\circ$  and  $\theta = 45^\circ$  planes.

approximately 2.8 m/s. Thus the total mass flow is greater than for the geometry of figure 1(a) but the ratio of the mass flow in the axial pipe to that in the primary radial jets is similar. Before comparing the two flows, it should be noted that the annulus geometry gives rise to differences between the  $0^\circ$  and  $45^\circ$  planes which are large and, in the upstream region, considerably larger than for the non-annulus geometry. The 0.75 m/s contour, for example, extends twice as far downstream in the  $45^\circ$  plane, and related circumferential variations are present in the annulus.

Comparison of figures 3 and 4 shows that, in keeping with the different trajectory angles of the primary jets, the primary vortex extends downstream of the axial plane of the radial jets to a value  $x/D = 1.2$ , rather than the value of 1.05 observed in the absence of the annulus. These figures correspond to a decrease in the trajectory angle of between  $15^\circ$  and  $20^\circ$ . The region of wall recirculation downstream of the primary jets, although not measured explicitly for the annular geometry, is clearly smaller in this case. Unlike the primary jets, the secondary jets do not penetrate to the centreline but do influence the centreline flow by reducing the axial velocity over a short region.

The results of figures 3 and 4, together with the measured results discussed in relation to the additional flow boundary conditions, provide information of direct relevance to gas turbine practice. In addition, they provide test cases against which the value of the calculation method, which is described in §3, can be determined. In the flow without the annulus, the calculation requires the specification of boundary conditions at, or close to, the exit planes of the baffle jet and of the radial jets. With the annulus, the boundary conditions are assigned in the same manner as in a real combustor, i.e. the flow rates to the baffle jet and to the annulus are known and can be converted, with simple assumptions, into the required velocity profiles. It is to be expected that the uncertainties involved in the specification of boundary conditions will be similar in the two cases, but the annulus geometry presents the added difficulty of requiring the calculation of the development of the velocity characteristics in the annulus and in the two sets of radial jets. The flow in the model combustor without the annulus should, therefore, be simpler to calculate.

### 3. Detail of calculations

Calculated results were obtained by solving the equations for conservation of mass and momentum in time-averaged uniform-property form, i.e.

$$\frac{\partial \bar{U}_i}{\partial x_i} = 0,$$

$$\bar{U}_j \frac{\partial \bar{U}_i}{\partial x_j} = -\frac{1}{\rho} \frac{\partial \bar{P}}{\partial x_i} + \frac{\partial}{\partial x_j} \left( \nu \frac{\partial \bar{U}_i}{\partial x_j} - \overline{u_i u_j} \right),$$

together with the equations corresponding to an eddy-viscosity turbulence-model closure and logarithmic wall functions. The turbulence model is represented by

$$-\overline{u_i u_j} = \nu_t \left( \frac{\partial \bar{U}_i}{\partial x_j} + \frac{\partial \bar{U}_j}{\partial x_i} \right) - \frac{2}{3} k \delta_{ij},$$

$$\nu_t = c_\mu k^2 / \epsilon,$$

$$\bar{U}_i \frac{\partial k}{\partial x_i} = \frac{\partial}{\partial x_i} \left( \frac{\nu_t}{\sigma_k} \frac{\partial k}{\partial x_i} \right) + \nu_t \frac{\partial \bar{U}_i}{\partial x_j} \left( \frac{\partial \bar{U}_i}{\partial x_j} + \frac{\partial \bar{U}_j}{\partial x_i} \right) - \left( \frac{\partial \bar{U}_i}{\partial x_j} \right)^2,$$

$$\bar{U}_i \frac{\partial \epsilon}{\partial x_i} = \frac{\partial}{\partial x_i} \left( \frac{\nu_t}{\sigma_\epsilon} \frac{\partial \epsilon}{\partial x_i} \right) + \frac{\epsilon}{k} \left[ c_1 \tau_t \frac{\partial \bar{U}_i}{\partial x_j} \left( \frac{\partial \bar{U}_i}{\partial x_j} \right) + \left( \frac{\partial \bar{U}_j}{\partial x_i} \right) - c_2 \epsilon \right],$$

with the constants

$$c_\mu = 0.09, \quad c_1 = 1.44, \quad c_2 = 1.92, \quad \sigma_k = 1.0, \quad \sigma_\epsilon = 1.3.$$

The six equations were solved in finite-difference form with the computer program PACE developed by Jones and described, for example, by Jones & McGuirk (1980*a, b*). The numerical formulation comprised a linearized, implicit, conservative scheme with central differencing except where the convective fluxes were large and the cell Reynolds number exceeded |2|: in such cases, donor-cell differencing was used. The equations were written in terms of the primitive variables velocity and pressure and the equation set solved by a guess-and-correct procedure similar to that of Chorin (1968) and others. The solution domains were represented as shown in figure 5 with boundary conditions assigned in the manner described in §§3.1 and 3.2 corresponding to the two model combustors. Wall functions, based on logarithmic near-wall behaviour of the mean velocity, were used to link the near-wall nodes to the wall, and are described, for example by Green (1981), Green & Whitelaw (1980), White (1980) and Jones & McGuirk (1980*a, b*).

#### 3.1. The non-annulus geometry

The symmetry of the non-annulus geometry allowed the restriction of the solution domain to a 90° sector with cyclic boundary conditions applied in two radial planes each at 45° to the axis of the jets. Flow boundary conditions were taken mainly from measurements; thus the mean-velocity and normal-stress values were measured 1.5 diameters upstream of the exit flows of the radial pipes. The known mass flow in the axial pipe was assumed to flow radially with uniform velocity in the circumferential plane of the baffle. Corresponding turbulent kinetic energy and dissipation rates were determined from the assumed mean-velocity profile with mixing-length assumptions: the influence of the turbulence assumptions was found to be negligible within a reasonable range. The solution domain extended to four chamber diameters down-

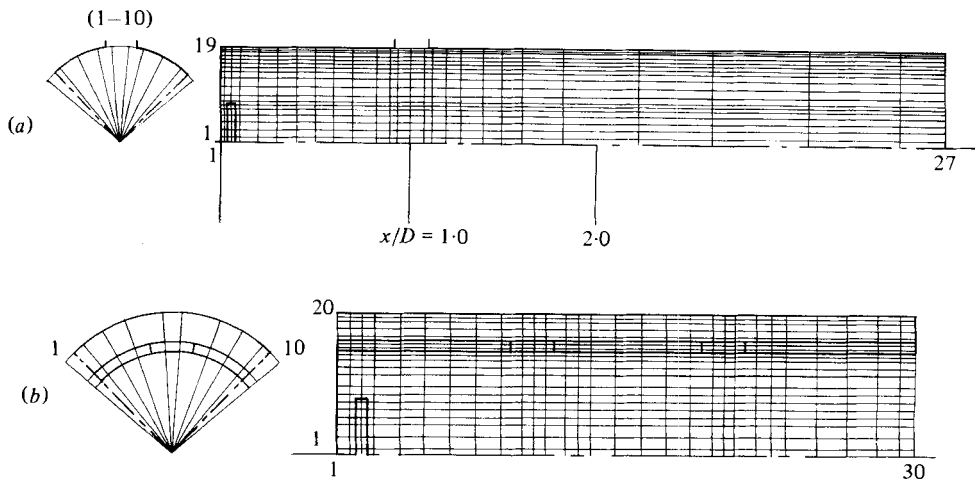


FIGURE 5. The finite-difference grids: (a) ( $10 \times 19 \times 27$  nodes) for the non-annulus geometry; (b) ( $10 \times 20 \times 30$  nodes) for the annulus geometry.

stream, where zero axial gradients of all dependent variables were assumed. The convergence criterion corresponded to residuals for each dependent variable of less than 0.2% and overall mass continuity of better than 0.5%.

The distribution of grid nodes used for the calculation of flows in the chamber of figure 1(a) is shown in figure 5(a) and corresponds to 5130 ( $27 \times 19 \times 10$ ) nodes. With this arrangement, about 400 iterations were required for the solution of the equations to converge. Present limitations on computer storage capacity and the high cost of computer time deny the possibility of extensive numerical tests with large numbers of grid nodes, and, as a consequence, the dependence of the solution on the chosen grid size cannot be completely established. However, confidence in the solutions may be obtained by assessment of the magnitude of truncation errors and by comparing the calculated and measured results.

An examination of the terms in the axial momentum equation within the region  $0.8 < x/D < 1.2$ , where the primary jets divide, shows that the convection and pressure-gradient terms are dominant and that the diffusion terms are up to two orders of magnitude smaller, except in the immediate vicinity of the stagnation region. Thus the flow in most of this region is pressure- rather than turbulence-controlled, and a paucity of grid nodes is likely to produce errors between calculations and measurements in high-pressure-gradient regions. This was found previously (Green & Whitelaw 1980) for a two-dimensional pressure-controlled flow where improvement resulted from increasing the number of grid nodes in regions of large pressure gradient; this is often less possible in the case of three-dimensional flows. Other errors associated with the calculation method, namely numerical diffusion and turbulence-model errors, can also be examined for the present solution.

The differencing scheme of the calculation method used either central differencing where the local cell Péclet number ( $Pe = U_i \Delta x / \nu_i$ ) was less than  $|2|$ , or upstream differencing where this criterion was not met, to determine the convection terms. Upstream differencing results in numerical diffusion (Roache 1976), which can smear the gradients of a variable and result in errors. The probable extent of numerical

Case	Zero velocity		Maximum velocity		Minimum velocity	
	measured	calculated	measured	calculated	measured	calculated
1	1.03	1.00	1.20	1.28	0.80	0.75
2	1.03	1.00	1.20	1.28	0.80	0.75
3	1.06	1.01	1.28	1.38	0.40	0.38

TABLE 1. Location  $x/D$  of measured and calculated velocities

diffusion in the present calculations was examined using a technique first employed by McGuirk & Rodi (1978) in which, *a posteriori*, an analysis was made of the solution using central differences and the imbalance in the momentum equation determined: this imbalance is a measure of the numerical diffusion. In the present flow, the effects of numerical diffusion in the important jet entry region were found to be small.

The above discussion suggests that numerical diffusion is not a major source of error except perhaps in the immediate vicinity of stagnation, where convection is unimportant. Unfortunately, turbulence assumptions may also be at fault here. The effects of a limited number of nodes on the calculation of pressure, for example, can be assessed from the previous two-dimensional calculation of Green & Whitelaw and could cause a significant but small shift in the location of the stagnation point, with consequent displacement of downstream profiles. It is clear that a study of stagnation regions of different flows would be useful to resolve the extent to which numerical and turbulence-model assumptions contribute to uncertainties in the calculated results. It can also be expected that the well-known inability of the two-equation model to represent streamline curvature and the approximations inherent in logarithmic wall functions will contribute to any discrepancies, but probably to a lesser extent than the numerical assumptions coupled with the limitations imposed on the number of nodes.

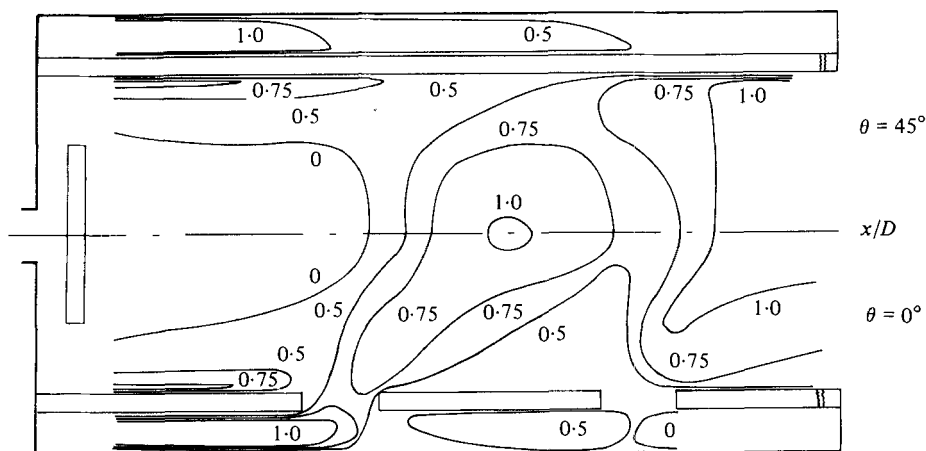
Figure 3 allows comparison of measured and calculated contours of mean axial velocity for the non-annulus geometry of figure 1(a), and it is clear that, in spite of the possible error sources discussed above, the agreement is more than adequate for engineering purposes, except perhaps for the jet-entry region  $0.8 < x/D < 1.4$ . The calculated centreline velocity at  $x/D = 1.2$  is 30% less than the measured value, but, although the magnitude of discrepancies between measured and calculated velocities is one criterion for judgement, another is the location of zero, maximum and minimum velocities, and table 1 indicates that the quality of agreement for this comparison is much better and of the order of the distance between nodes.

### 3.2. The annulus geometry

The boundary conditions for the second geometry were again taken mainly from measurements. The radial flow from the baffle entry was treated as for the previous geometry, but the boundary conditions for the primary and secondary flows were specified in the annulus at  $x/D = 0$ ; consequently the finite-difference grid was increased to 6000 ( $30 \times 20 \times 10$ ) nodes to encompass both the main tube and the annulus (figure 5b). This resulted in an increase in the number of iterations to about 700 to achieve the same state of convergence as the previous calculation. The increase in the number of iterations was due to the destabilizing effect of solving the equations with internal walls containing only small areas, i.e. the primary and secondary holes,

Number of nodes in primary hole	Ratio of mean flow through primary holes to that in upstream annulus	Initial jet angle
2	0.331	62.3°
6	0.445	69.1°
12	0.451	69.1°

TABLE 2. Influence of number of nodes in hole

FIGURE 6. Calculated mean axial velocity contours for  $\theta = 0^\circ$  and  $\theta = 45^\circ$  planes.

where the solution in the annulus and the main tube is linked. In addition, the division of mass flow through the primary and secondary holes had to be determined by the calculation procedure.

Owing to the limitations of the cylindrical polar co-ordinate system, the primary and secondary holes were assumed to be square, with areas equal to those of the circular holes in the experimental model. The detailed study of combustor-port configurations by Dittrich (1958) showed that the difference between the discharge coefficients for square and round holes is less than 1% for a wide range of annulus flow rates. The number of nodes required to represent the flow in the square holes was unknown and numerical experiments were performed, with typical results given in table 2. Here the jet angle is defined as the inverse tangent of the ratio of the average radial to axial velocity in the exit plane of the hole. The results show very small differences for 6 to 12 nodes and, of the 6000 nodes used for the results of the following paragraphs, 6 were assigned to each of the primary and secondary holes.

Calculated contours of mean axial velocity are shown in figure 6 for both  $0^\circ$  and  $45^\circ$  planes; these may be compared with the measured contours (figure 4) to gain an overall impression of agreement. The quality of agreement is similar to that shown for the previous calculations, although in some regions, for example at  $x/D = 1.4$ , the centreline velocity is underpredicted by 40%. This worsening of agreement can be attributed mainly to the calculated proportions of primary- and secondary-hole flow. Whereas the flow distribution in the experimental model was approximately equal between primary and secondary holes, only 40–45% of the total flow entered

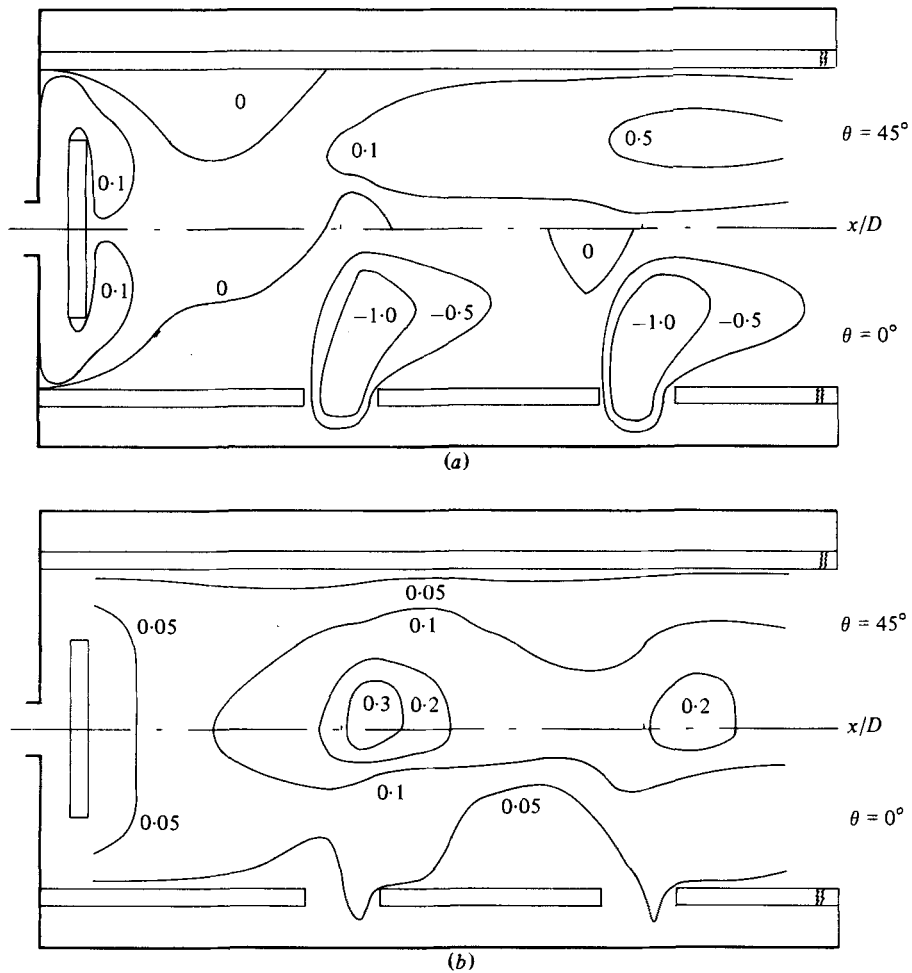


FIGURE 7. (a) Calculated mean radial velocity contours for  $\theta = 0^\circ$  and  $\theta = 45^\circ$  planes. (b) Calculated turbulence kinetic energy contours for  $\theta = 0^\circ$  and  $\theta = 45^\circ$  planes.

the primary holes in the calculations. This resulted in the prediction of lower centreline velocities in the region  $1.0 < x/D < 2.0$  and higher velocities in the zero-degree plane just downstream of the secondary holes. The spreading rate of the square jets and the resulting impingement, in the case of the primary jets, also contributed to errors in the calculated distribution of the flow.

The overall agreement is, however, satisfactory, and provides a basis for parametric studies of the influence of geometrical or flow-inlet conditions such as those described in §3.3. The calculated contours of mean radial velocity are presented in figure 7(a) and correspond to the mean axial velocity of figure 4. In the zero-degree plane it can be seen that the primary jets impinge on the centreline to cause a region of negative radial velocity in the  $45^\circ$  plane. Further downstream, however, the secondary jets do not impinge on the centreline. The contours of kinetic energy, shown on figure 7(b), indicate the main regions of turbulence generation that are necessary to ensure rapid mixing of fuel and air in the primary region and rapid dilution and cooling in the secondary region. In common with measurements of axial normal stress, the

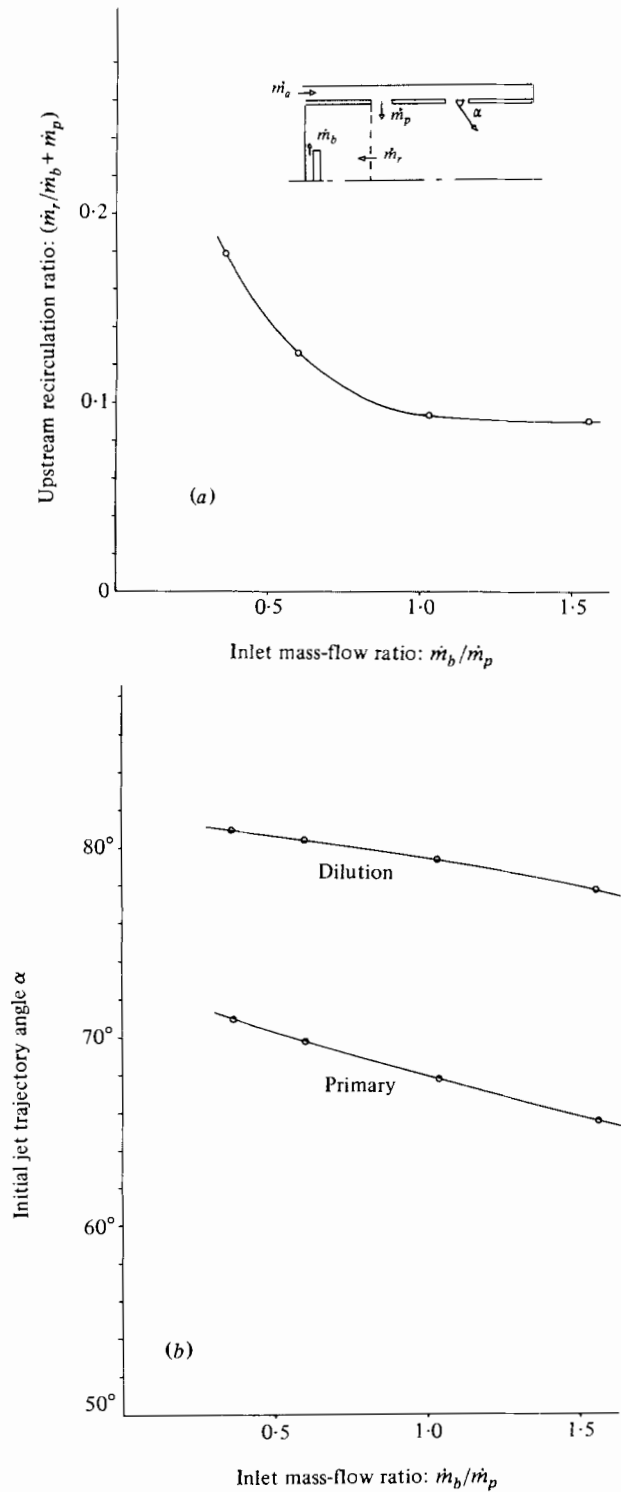


FIGURE 8. (a) Relationship between upstream recirculation ratio and inlet mass-flow ratio. (b) Relationship between initial jet-trajectory angle and inlet mass-flow ratio.

highest values of kinetic energy occur close to the centreline and in the region of negative mean radial velocity.

### 3.3. Further calculations

With the limitations of §3.2 in mind, the calculation method was used to quantify the effect of variables that could be determined by experiment but at greater inconvenience and cost. Figure 8(a) demonstrates the ratio of the primary-jet fluid that enters the primary zone of the annulus geometry to the total primary mass flow as a function of the primary-inlet mass-flow ratio. This parameter is important in practice, since it helps to determine the strength of the air-fuel mixture in the primary zone of combustors, and hence the efficiency and emissions performance. Although the length of the primary vortex does not change with the present arrangement, the results of figure 8(a) show a rapid and nonlinear reduction in the proportion of primary air entering the primary vortex as the main-flow ratio is reduced. The absolute magnitude of the calculated results must be regarded as approximate, but the trend is likely to be correct. In gas-turbine practice, manufacturing tolerances would in any case render any measured representation of the same effect as approximate. It should be emphasized that the present results relate to an idealized geometry and that they are likely to vary from one arrangement to another, and particularly with the arrangement for supplying the fluid to the head of the combustor and with the number of primary holes.

Another important aspect of combustor design is the injection angle of the primary jet, which has an influence on combustion efficiency and pollution emission as a consequence mainly of its influence on the proportion of the jets which enter the primary zone. Calculated jet trajectory angles are shown on figure 8(b) for the primary and secondary jets, as they enter the main tube, as a function of the primary-inlet main-flow ratio. The decrease in jet angle with increase in mass-flow ratio is similar for both primary and secondary jets, and is in contrast to the non-annulus geometry, which provides a nearly constant primary jet angle of  $90^\circ$ .

## 4. Concluding remarks

The qualitative prediction of the overall flows in isothermal combustor models has been shown to be feasible, and the calculation method may be applied to parametric studies to facilitate initial design specifications. Exact quantitative agreement between measurement and calculations is, however, subject to limitations imposed by the assumed numerical and turbulence models and by economic factors. The observed discrepancies are larger than those found in the calculation of single jets, for example, by Jones & McGuirk (1980*b*) and White (1980); but only by a small amount, and this is to be expected since the primary jets in the present case divide to contribute fluid to the upstream flow.

In three-dimensional calculations, where the flow includes regions of recirculation, it is unlikely that either computer storage capacity or computer-time costs will presently allow sufficiently large grid distributions to ensure grid independence of the solution. Careful examination of the solution is required for signs of numerical diffusion, and errors are to be expected, though not always of serious magnitude, in these regions of strong streamline curvature, or in the vicinity of stagnation or separation where the two-equation turbulence model is invalid. The axial momentum equation was shown to be dominated by convection and pressure-gradient terms with relatively small numerical diffusion in those regions having a strong influence on the

flow upstream and downstream, i.e.  $0.8 < x/D < 1.2$ . It is worth noting that, in calculations involving combustion as might be attempted later in the design process, the equations for temperature or chemical species could be subject to numerical diffusion in these regions since they do not have a pressure-gradient or equivalent dominant source term.

The most useful application of the calculation method at the present time is for parametric studies that require trends, rather than absolute values of the dependent variables. The assembly of information of this type requires a lengthy and expensive process using traditional experimental techniques, and may be more readily and cheaply accomplished by calculation.

The authors gratefully acknowledge financial support from the Ministry of Defence and many useful discussions with colleagues at Imperial College, The National Gas Turbine Establishment and Rolls-Royce. Dr D. Dryburgh provided helpful comments on the original manuscript and particularly on those aspects that relate to real combustors.

#### REFERENCES

- CHORIN, A. J. 1968 Numerical solution of the Navier–Stokes equations. *Math. Comp.* **22**, 000.
- DITTRICH, R. T. 1958 Discharge coefficients for combustor–liner–air-entry holes. *NACA TN 3924*.
- DURST, F., MELLING, A. & WHITELAW, J. H. 1981 *Principles and Practice of Laser-Doppler Anemometry*, 2nd edn. Academic.
- GREEN, A. S. 1981 Isothermal models of combustion chamber flows. Ph.D. thesis, University of London.
- GREEN, A. S. & WHITELAW, J. H. 1980 Measurement and calculations of the isothermal flow in axisymmetric models of combustor geometries. *J. Mech. Engng Sci.* **22**, 119.
- HARSHA, P. T. 1981 Combustion modelling for practical applications. In *Proc. Session on Prediction of Turbulent Reacting Flows in Practical Systems*. A.S.M.E.
- JONES, W. P. & MCGUIRK, J. J. 1980a Mathematical modelling of gas turbine combustion chambers. *AGARD CP275*, Paper 4.
- JONES, W. P. & MCGUIRK, J. J. 1980b Computation of a round jet discharging into a confined mass flow. In *Turbulent Shear Flows 2* (ed. L. J. S. Bradbury, F. Durst, B. E. Launder, F. W. Schmidt & J. H. Whitelaw), p. 233. Springer.
- JONES, W. P. & WHITELAW, J. H. 1982 Calculation methods for reacting turbulent flows: a review. To be published in *Combust. & Flame*.
- LIBBY, P. A. & WILLIAMS, F. 1980 *Turbulent Reacting Flows*. Springer.
- MCGUIRK, J. J. & RODI, W. 1978 A depth-averaged mathematical model for the near field of side discharges into open-channel flow. *J. Fluid Mech.* **86**, 761.
- ROACHE, P. J. 1976 *Computational Fluid Dynamics*. Hermosa.
- WHITE, A. J. 1980 The predictions of the flow and heat transfer in the vicinity of a jet in crossflow. *A.S.M.E. Paper 80-WA/HT-26*.